Experimental Animals
Exp. Anim. 73(4), 399–411, 2024

Original

Resistance against the development of diethylnitrosamine-induced hepatocellular carcinoma in female C3H mice: an experimental model

Daniela Romina MONTAGNA[1)], María Florencia TODERO[1)], Gabriela Cintia POSTMA[2)], Roberto TRIGO[2)], Alan BERNAL[1)], Oscar BUSTUOABAD[1)], Mónica VERMEULEN[1)], Raúl RUGGIERO[1)]* and Alejandra DUARTE[1,3)]*

[1)]*Instituto de Medicina Experimental (IMEX-CONICET), Academia Nacional de Medicina de Buenos Aires, Pacheco de Melo 3081, 1425, Buenos Aires, Argentina*
[2)]*University of Buenos Aires, Faculty of Veterinary Sciences, Department of Pathology, Avenue Chorroarin 280, C1427CWO, Argentina*
[3)]*Fundación Héctor Alejandro (H.A.) Barceló, Instituto Universitario de Ciencias de la Salud, Larrea 770, C1030AAP, Buenos Aires, Argentina*

Abstract: Histopathological features of hepatocellular carcinoma (HCC) induced by diethylnitrosamine (DEN) in mice display strong similarities with those seen in humans, including the higher tumor prevalence in males than in females. Previous studies have demonstrated that continual production of the pro-inflammatory IL-6 by Kupffer cells is involved in the initiation and progression of DEN-induced HCC and that estrogen-mediated reduction of IL-6 secretion would decrease its incidence in females. Given the predominant utilization of male mice in hepatic carcinogenesis research, the objective of this study was to examine histopathological and immunological parameters in the DEN-induced liver carcinogenesis model in female C3H mice. We observed a significant prevalence of hepatocellular hyperplasias and adenomas alongside a minimal infiltration of inflammatory cells and a scarcity of senescent areas in females. Further, a low expression of immunosuppression markers is observed in females − such as neutrophil/lymphocyte ratio, PD-1 expression in CD8 T cells, and PD-L1 in myeloid cells − compared to males. Comparative studies between susceptible and resistant hosts to chemical carcinogenesis may help to unveil novel therapeutic strategies against cancer.
Key words: animal models, cancer, immunology, liver diseases, mice

Introduction

The histology and genetic signature of hepatocellular carcinoma (HCC) induced by diethylnitrosamine (DEN) in mice are strongly similar to those seen in humans [1, 2]. Another point of resemblance is the higher incidence and faster HCC tumor growth observed in males compared to females in both animal and clinical settings [3–5].

Estrogen-mediated protective effects were reported against liver cancer in female mice, while the male sex hormone testosterone has been implicated in contributing to HCC development [6].

In terms of tumor growth and progression, male mice often exhibit aggressive HCC with larger tumor sizes, faster rates of tumor growth, and pro-inflammatory immune response, potentially influenced by hormonal, genetic, and immune factors. Conversely, female mice demonstrate a more balanced immune response, potentially influenced by more efficient immune surveillance mechanisms. Additionally, differences in liver metabo-

(Received 27 October 2023 / Accepted 24 May 2024 / Published online in J-STAGE 3 August 2024)
Corresponding author: D.R. Montagna. email: daniela.r.montagna@gmail.com
**These authors contributed equally to this research.*
Supplementary Figures: refer to J-STAGE: https://www.jstage.jst.go.jp/browse/expanim

lism and detoxification pathways between males and females may contribute to variations in HCC development [7–10].

Former studies have demonstrated that continual production of the strong pro-inflammatory cytokine IL-6 by Kupffer cells is involved in the development of DEN-induced HCC and that estrogen-mediated reduction of IL-6 secretion would decrease its incidence in mouse females [1, 8–11].

DEN-induced HCC in male mice has been used extensively in search of experimental models with a high and uniform incidence of tumors, with less variability among the pathophysiological parameters to be studied. However, these sex-specific differences highlight the importance of considering sex as a biological variable in cancer research, offering potential insights for targeted therapeutic interventions [1, 7].

Given the predominant utilization of male mice in hepatic carcinogenesis research, the objective of this study was to examine histopathological and immunological parameters in the DEN-induced liver carcinogenesis model in female C3H mice.

This research addresses the gap in understanding hepatic tumor development in female mice, providing insights for future studies on HCC.

Material and Methods

Experimental animals

Female and male C3H/HeJ mice were bred in *Comisión Nacional de Energía Atómica*, Argentina. They were used from 15 days up to, in some cases, 315 days of age. Animals were housed in the Instituto de Medicina Experimental (IMEX-CONICET), Academia Nacional de Medicina facilities in Buenos Aires. The Committee for the Care and Use of Laboratory Animals (CICUAL) of IMEX-CONICET approved all experimental procedures (protocol N°087/2021). The experiments' performance complies with the Directive EU63/2010.

DEN-induced HCC model

A single intraperitoneal (i.p) injection of DEN (Sigma-Aldrich N0258, St. Louis, MO, USA) was administered at 10 mg/kg body weight in both female and male C3H mice at 2 weeks old to induce hepatic tumor formation. The drug was diluted in a physiological solution, with a total volume of 0.1 ml and a 30 G needle. Mice were not weaned (they continued to lactate after inoculation until conventional weaning). The inoculation did not cause lesions or profound clinical impact in mice, except for a record of transient weight loss that, over the days, was reversed. Animals were periodically monitored and provided with accessible water-soaked pellets to ensure correct feeding after weaning. The body weight of the animals was regularly measured [1, 2].

As previously described, after mice receive a single injection of DEN at 15 days of age, the first microscopic tumor foci appear in the liver about 90 days after DEN administration, and macroscopic nodules are already evident 210 days post-DEN [1, 10]. The percentage of HCC and the number of tumor foci per liver are significantly higher in males than in females [3, 4, 12].

Study design

The experimental unit is a mouse. Two groups of female mice and two groups of male mice were inoculated with one dose of the carcinogen DEN at 15 days old. Control groups of female and male mice were injected with 0.1 ml of saline solution i.p. at the same age as a carcinogen. Control and DEN-treated mice were subjected to euthanasia 210 and 300 days after the administration of the carcinogen.

Sample size

The n per group was 5 experimental units (except the male control group of 7 experimental units). n total=42. The calculation of the sample size a priori was carried out with an effect size of 0.7, a 1-β=0.8, and α=0.05. The variable considered was the number of tumor foci/liver. No experimental units have been excluded from the analysis. The results are mainly focused on the comparison between female and male mice post-administration of the carcinogen at each described time.

Randomization and blinding

Randomization was done using the Rand formula (Excel software). All experimental procedures were carried out blindly and according to ARRIVE guidelines.

Humane endpoint criteria

Criteria established for the experimental endpoint were: degree of dehydration greater than 5% (assessed by the skinfold test and hydration of the ocular mucosa), decreased mobility, moderate to severe ascites, decreased body weight greater than 15% (corresponding to a body score less than or equal to 2/5) and non-reversible signs of pain with the administration of tramadol 5 mg/kg subcutaneously (s.c.). However, mice did not present signs of alterations in their clinical parameters during the development of the experiment, that is, until day 300 after the DEN inoculation when the last groups were euthanized.

Severity of the procedure: moderate [1, 13].

Extraction of samples

A blood sample was taken on day 45 post-DEN through the submandibular vein. Then, at 210- and 300-days post-DEN, mice were anesthetized with ketamine (80 mg/kg) + xylazine (7 mg/kg) in a single i.p. inoculation (0.1 ml) diluted in sterile physiological solution for blood collection, mesenteric lymph nodes, bone marrow, spleen, and liver obtaining as applicable. The anesthetic state was evaluated by: loss of the station, palpebral reflex, corneal reflex, and absence of foot, tail, and ear reflexes. In addition, the respiratory pattern was monitored. Subsequently, terminal blood collection through cardiac puncture was performed, and immediately, they were euthanized by cervical dislocation. After euthanasia, organs were removed for the *ex vivo* studies detailed below.

Collection and processing of tissue samples

Hemogram: Blood samples were obtained by submandibular puncture in heparinized tubes or by cardiac puncture before euthanasia. Blood cell count was performed using the hematology analyzer Abacus Junior Vet (Diatron, Medley, FL, USA).

Biochemical parameters: Enzymes alanine aminotransferase (ALT/GPT) and aspartate aminotransferase (AST/GOT) were measured in serum with a commercially available kit from Wiener Lab (Buenos Aires, Argentina) according to the manufacturer's instructions (MINDRAY BS-200E clinical chemistry autoanalyzer).

Liver analysis: Livers were weighed, and the number of visible nodules on the liver surface were counted macroscopically. Liver tissue was removed and hepatocytes were dispersed in RPMI medium to create a single-cell suspension. Cells were lysed by four freeze cycles (on liquid nitrogen) and thaw cycles. Larger particles were removed by centrifugation, supernatants were sonicated for 10 min in a Branson Digital SoniWer (Sonifier, Brookfield, CT, USA), protein content was determined and adjusted at 7.5 g/ml, and aliquots were stored at −80°C until use.

Histological analyses: Livers were fixed in 10% PBS-formaldehyde. Five serial sections of representative lesions from each liver were obtained and stained with hematoxylin and eosin. Sections were evaluated for signs of malignancies by an experienced and blinded pathologist. Ten fields per section were analyzed. In each field, the presence of the characteristics (cellular atypia, distorted architecture, and necrosis) was evaluated. The results were expressed as the percentage of occurrence of each characteristic per analyzed section of each evaluated representative hepatic lesion. Ten fields were also evaluated for mitotic and Kupfer cell counts. Liver injuries were classified according to the International Harmonization of Nomenclature and Diagnostic Criteria for Lesions in Rats and Mice (INHAND) guidelines [14, 15].

Senescence analysis: The evaluation of senescence was performed by β-galactosidase staining (Senescence Detection Kit, Biovision, Zurich, Switzerland) [16].

Immunofluorescence: Livers were frozen with dry ice and maintained at −80°C. Serial sections (3–5 μm) were obtained with cryostat. The immunofluorescence was performed as previously reported [12, 14]. Briefly, the tissues were rehydrated with PBS and fixed with 4% paraformaldehyde in PBS for 10 min at room temperature. After sections were blocked with a solution of 3% bovine serum albumin (BSA) for 30 min at RT. Sections were incubated with the antibodies for 2 h at 4°C RT (Anti-CD8-FITC with anti-PD-1-PE or anti-F480-FITC with anti-PDL1-PE − anti-mouse monoclonal antibodies (Ap-Biotech, Quilmes, Argentina), all at 1:250 dilutions). After several washes, coverslips were mounted onto the slides using Fluorsave antifade reagent (Calbiochem, St. Louis, MO, USA) followed by examination using a Zeiss LSM 510 laser-scanning confocal microscopy. Signal overlap was quantified using MBF-Image J and Pearsons colocalization coefficients were calculated.

Cell suspensions of spleen and lymph nodes: Spleens and mesenteric lymph nodes were removed and passed through sterile mesh with PBS supplemented with 5% FBS, 1% penicillin, and 1% streptomycin to obtain a single-cell suspension. Erythrocytes were eliminated with a red blood cell lysis buffer (NH_4Cl 0.15 M; $NaHCO_3$ 10 mM; EDTA 0.1 mM; pH 7.3), and cells were washed and counted with trypan blue dye.

Bone marrow-derived dendritic cell culture: The femurs of mice were removed and freed of muscles and tendons. Both femur ends were cut off and the marrow was flushed out with RPMI 1640 medium. Erythrocytes were lysed with ammonium chloride (0.45 M). Cells were cultured as previously reported [17].

Cytokine measurements: IL-6, IL-1β, and INF-γ were measured by ELISA kits (R&D Systems, Minneapolis, MN, USA), according to the manufacturer's recommendations.

Flow cytometry: Anti-CD11c (PE-Cy5), anti-IAb (PE), anti-CD86 (FITC), anti-CD4 (FITC), anti-CD8 (PE), anti-B220 (FITC), anti-CD19 (PE-Cy5), anti-CD11b (FITC), anti-GR1 (PE), anti-F480 (FITC), anti-PD-1 (PE), and anti-PD-L1 − clone MIH5 (PE) − anti-mouse monoclonal antibodies (Ap-Biotech) were used to assess the characteristics of splenocytes, mesenteric lymph node cells, peritoneal macrophages, and bone marrow-derived dendritic cells by flow cytometry. Per-

centage and fluorescence of individual cells were measured in a flow cytometer (Becton Dickinson, Franklin Lakes, NJ, USA) and analyzed by Flowing (Software version 2.5.1, Turku Centre for Biotechnology, University of Turku, Turku, Finland) [14, 18].

Proliferation assays: Lymphocyte proliferation was evaluated by CFSE staining (Molecular Probes, Eugene, OR, USA). Briefly, 1×10^7 cells/ml were suspended in 0.3% BSA/PBS. Then, 1 μl of CFSE was added for each ml (0.5 μM) (Invitrogen, Waltham, MA, USA) and cells were incubated for 15 min at 37°C. Cells were washed three times with complete RPMI and incubated for 5 min at 37°C between washes. Afterward, 1×10^5 lymphocytes were cultured in 96-well flat-bottom plates for 72 h in the presence or absence of 5 μl/ml of concanavalin A (CoA).

Statistical analysis

GraphPad PrismSoftware® performed the statistical analysis. Student's *t*-test or analysis of variance (ANOVA) followed by the Tukey test were used as appropriate. Values were expressed as mean ± SE. Differences were considered to be significant whenever the *P*-value was less than 0.05.

Results

Development of liver tumors induced by DEN in female and male C3H mice

As previously reported, a lower susceptibility to the carcinogen DEN was observed for the development of liver tumors in C3H females than in males [6–9]. The number of macroscopic hepatic nodules was significantly lower in females compared to males, both on day 210 and day 300 post-DEN administration. At day 210 post-DEN, two out of five female C3H mice exhibited macroscopic liver nodules, while at day 300 post-DEN, nodules were observed in four out of five female C3H mice. On the contrary, at both day 210 and day 300 post-DEN, macroscopic liver nodules were evident in all five male C3H mice in each respective period (Fig. 1a). Accordingly, liver/mouse weight ratio was significantly lower in DEN-treated females (Fig. 1b).

On day 210 post-DEN administration, histological analysis revealed that 40% of females developed hyperplasia, while 60% showed no histological lesions (Figs. 1c and d). In contrast, during the same period, 80% of male mice developed adenomas, with the remaining 20% showing hyperplasia (Supplementary Fig. 1). The hepatic hyperplasia observed in female mice exhibited small-sized nuclei with clumped chromatin. Vacuolated cytoplasm containing basophilic material was predominant, with no mitotic figures detected (Fig. 1e and f).

At day 300 post-DEN administration, 40% of females displayed hyperplasia, while an additional 40% developed adenomas (Figs. 1c and d). Interestingly, one female exhibited a significant tumor mass diagnosed as a diffuse well-differentiated hepatocellular carcinoma, representing the remaining 20% of females. This observation highlights the notable variability in liver lesions among DEN-treated females, as illustrated in Supplementary Fig. 2. Conversely, 100% of male mice developed HCC (Supplementary Fig. 1).

Adenomas in females, at day 300 post-DEN administration, showed variable nuclear sizes and occasional binucleated cells. The cytoplasm was vacuolated with basophilic material, and mitotic activity was low. Nodules exert compressive effects on adjacent parenchyma. Congested blood vessels and a small number of inflammatory cells, mainly Kupffer cells, were observed in sinusoids (Figs. 1e, f, and Supplementary Fig. 3). The presence of cellular atypia and distorted architecture in the livers of male treated mice was significantly higher than in females, both at day 210 and day 300 post-application of DEN. The presence of necrosis was significantly higher in males than in females starting from day 300 post-DEN (Fig. 1c, Supplementary Figs. 1c and 3). Histological examination of control groups revealed no significant changes in males and females euthanized at days 210 and 300, respectively (Supplementary Fig. 3).

Differential liver damage in females and males treated with DEN

In females treated with DEN, IL-6 levels in the liver remain low at both days 210 and 300 (Fig. 2a), correlating with a minimally distorted hepatic architecture compared to males. In contrast, males exhibit higher IL-6 values over time. It is important to note that untreated female mice consistently showed low levels of IL-6 throughout aging, unlike males (Supplementary Fig. 4).

On the other hand, no significant differences were observed in the levels of IL-1β in the liver (Fig. 2b), and IL1-β was undetectable in the serum of males and females (data not shown).

In addition, we observed a low percentage of senescent areas in the livers of DEN-treated females (Fig. 2d). Senescent areas were more extensive in males, related to the higher concentration of IL-6 observed in both serum and liver, which is part of the senescence-associated secretory phenotype (SASP).

In agreement with the above, DEN-treated female mice exhibited lower serum IL-6 concentrations compared to males, with this difference becoming signifi-

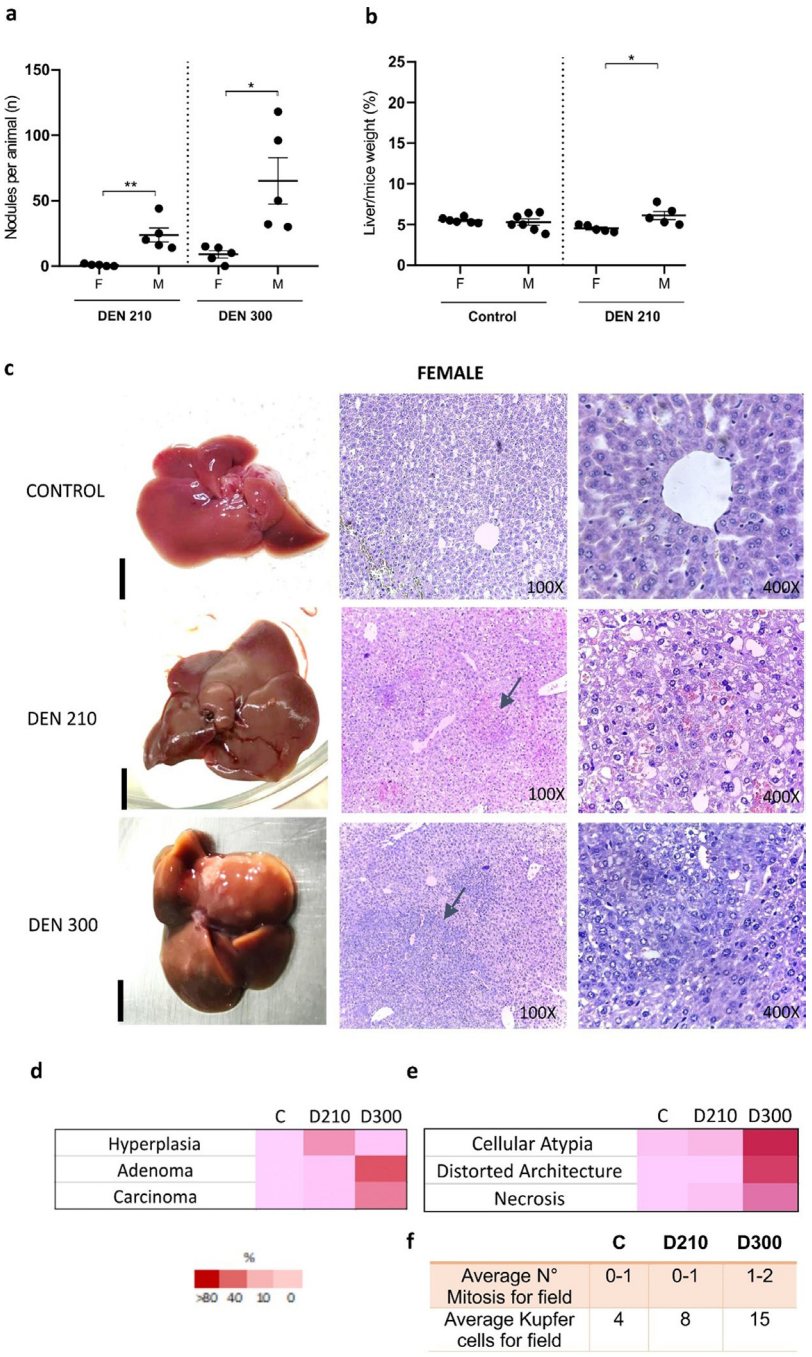

Fig. 1. Development of liver tumors induced by diethylnitrosamine (DEN) in female C3H mice 210- and 300-days post-DEN. (a) Number of macroscopic nodules per animal at 210- and 300-days post-DEN. Nodules at the surface of each lobe were counted using a microscope (black bars: 5 mm). Data represent the mean ± SEM of nodules per liver (n) of 5–7 mice per group. (b) Percentage of liver weight concerning weight (%) of control mice and DEN-treated mice 210 and 300 days after inoculation. Data represent the mean ± SEM of weight (%) of 5–7 mice per group. Statistical comparison among experimental groups: *P<0.05; **P<0.02; ***P<0.01. ANOVA followed by the Tukey test was used. (c) Representative macroscopic and histopathological images of female control and DEN-treated mice 210 and 300 days after inoculation. Haematoxylin and eosin (H&E) staining, 100 and 400×. Day 210 post DEN: the image shows hepatic hyperplasia (arrows, 100×). The nuclei appear small and contain clumped chromatin. The cytoplasm displays vacuoles and primarily exhibits basophilic material (400×). Day 300 post DEN: the image shows hepatic adenoma, which exerts compressive effects on adjacent parenchyma. (arrows, 100×). Note the presence of variable nuclear sizes and occasional binucleated cells. The cytoplasm is vacuolated with basophilic material. (d) Heat map represents the percentages of hyperplasias, adenomas, and carcinomas diagnosed within each experimental group of females, including controls, and at days 210 and 300 post-DEN treatment. (e) Detailed information on the degree of cellular atypia, distortion of liver architecture, and necrosis in DEN-treated females. The heat map indicates a semiquantitative analysis of the respective liver histologic features, ranging from faint red (not present) to dark red (a feature present in all/almost all liver sections). (f) Average numerical values for mitosis and Kupffer cells per field. Ten fields per liver were analyzed. Due to the lack of significant histological changes observed in the control groups euthanized on day 210 and day 300, the data from the controls on day 210 is depicted in the figure for simplification purposes.

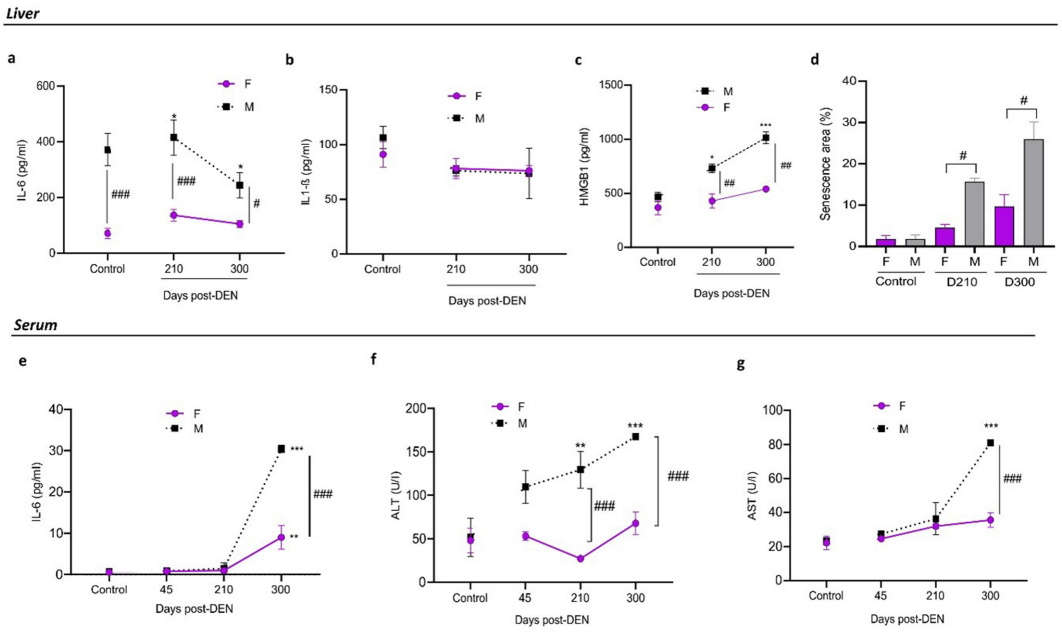

Fig. 2. Hepatic functional parameters and senescence in female and male diethylnitrosamine (DEN)-treated mice. (a, e) The concentration of IL-6 (pg/ml) in liver lysates (a) and serum (e) from control and DEN-treated mice was evaluated by ELISA assay. (b) Concentration of IL-1β in liver lysates. Levels of IL-1β in serum were undetectable. (c) Concentration of HMGB1 in liver lysates. Data represent the mean ± SEM of IL-6, IL-1β, or HMGB1 of 5 mice per group. Statistical comparison between experimental groups and control: $^{*}P<0.05$; $^{**}P<0.01$; $^{***}P<0.001$. Statistical comparison among female and male groups at the same time: $^{\#}P<0.05$; $^{\#\#\#}P<0.001$. (d) Percentage (%) of senescence in liver sections of female and male DEN-treated mice at 210-, and 300-days post–DEN administration. Data represent the mean ± SEM of senescence areas (%) per liver section of 5 mice per group. Statistical comparison among female and male groups at the same time: $^{\#}P<0.05$. (f) Alanine aminotransferase (ALT) and (g) aspartate aminotransferase (AST) levels (U/I) in the serum of control mice and mice treated with DEN. Data represent the mean ± SEM of ALT or AST levels of 5 mice per group. Statistical comparison among experimental groups: $^{**}P<0.01$; $^{***}P<0.001$. Statistical comparison among female and male groups at the same time: $^{\#\#\#}P<0.001$. All statistical analyses of this figure were performed using ANOVA followed by the Tukey test. F=female; M=male. The control group corresponds to day 210.

cantly evident at day 300 post-DEN (Fig. 2e), in line with the histological characteristics observed at that time.

Similarly, hepatic levels of HMGB1 were significantly lower in females than in males (Fig. 2C). Regarding liver function, DEN-treated female mice exhibited lower serum concentrations of alanine aminotransferase (ALT) and aspartate aminotransferase (AST) compared to males, with values remaining constant over time (Figs. 2f and g).

Immune response in female mice treated with DEN

In order to evaluate the immune response associated with the low proportion of HCC observed in DEN-treated female mice, blood samples were drawn at different times after DEN inoculation. Monocyte (Fig. 3a) and lymphocyte counts (Fig. 3b) were higher, and neutrophil count (Fig. 3c) was lower in DEN-treated females than in males from day 210 onwards after DEN administration. Overall, neutrophil-to-lymphocyte ratio (NLR), was significantly lower in females (Fig. 3d).

Splenic CD4 T lymphocytes count was lower in females than in males at day 210 post-DEN (Fig. 4a). No significant differences between sexes were observed in mesenteric lymph node CD4 T lymphocytes counts (Fig. 4b) nor in CD4 T surface expression of PD-1 (not shown).

On the other hand, a higher number of splenic and mesenteric lymph node CD8 T lymphocytes were observed in males than in females at day 300 post-DEN (Figs. 4c and d). Nevertheless, mesenteric lymph node CD8 T lymphocytes of females displayed a higher rate of proliferation (Fig. 4e), a higher INFγ secretion (Fig. 4f), and lower expression of surface PD-1 than males (Fig. 4g). No significant differences between sexes have been observed in the expression of PD-1 in splenic CD8 T cells (data not shown). Consistently, livers from female DEN-treated mice showed decreased CD8 T lymphocytes infiltrate (Fig. 4h), with lower expression of PD-1 than males (Fig. 4i).

 doi: 10.1538/expanim.23-0149

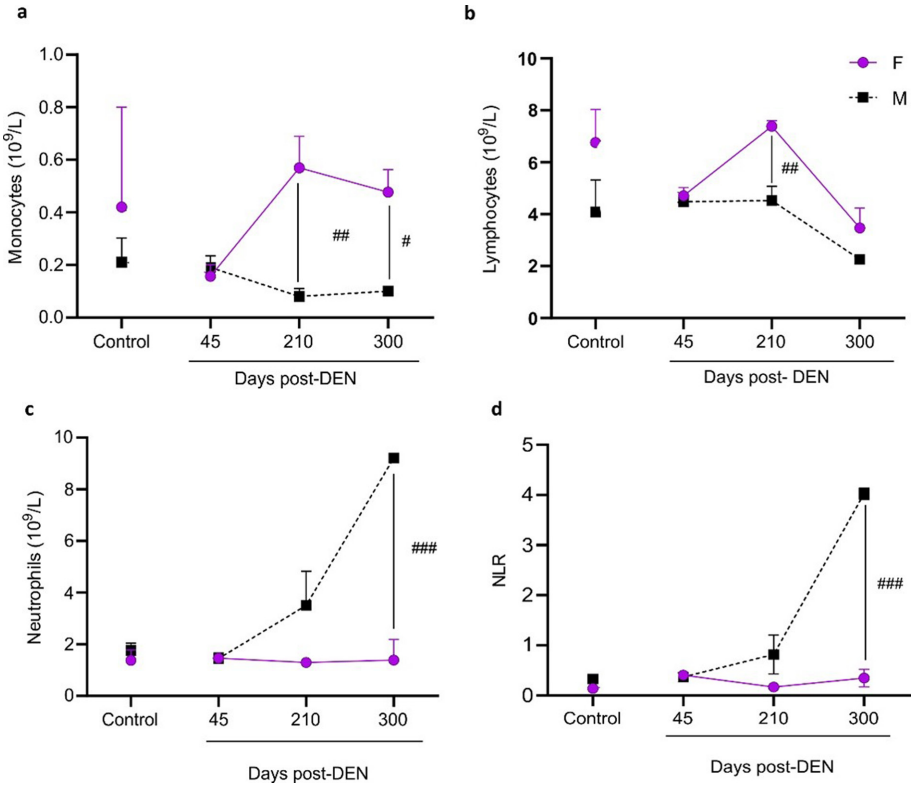

Fig. 3. Blood cell count of females and male diethylnitrosamine (DEN) − treated C3H mice. Count of monocytes (a), lymphocytes (b), neutrophils (c), and neutrophil-to-lymphocyte ratio (NLR) (d). Data were expressed as mean (10^9/L) ± SEM of cell number. Statistical comparison among female and male groups at the same time: $^{\#}P<0.05$; $^{\#\#}P<0.01$; $^{\#\#\#}P<0.001$. All statistical analyses of this figure were performed using ANOVA followed by the Tukey test. Due to the lack of significant changes observed in the control groups euthanized on day 210 and day 300, the data from the controls on day 210 is depicted in the figure for simplification purposes.

Subsequent analyses were conducted at day 210 after the administration of DEN, given the significant differences observed in lymphocyte populations from this time point onwards. Furthermore, day 210 represents a time point before tumor progression to HCC; thus, the observed changes at this time are not yet a consequence of HCC development, but rather precede its establishment.

Livers from DEN-treated females showed decreased macrophage infiltrate (Fig. 5a), with lower expression of PD-L1 than males (Fig. 5b). In addition, a decreased number of macrophages displaying a lower expression of PD-L1 was observed in females in the spleen (Figs. 5c and d), lymph nodes (Figs. 5e and f), and peritoneum (Figs. 5g and h).

In the same way, mesenteric lymph nodes and spleens B lymphocytes from DEN-treated female mice showed lower PD-L1 expression than males (Figs. 6a–d).

DC maturation markers CD86 and MHC II were not affected in the presence of lysates from DEN-treated female livers. However, a decrease in DC maturation was observed with liver lysates from DEN-treated males (Figs. 6e and f).

Discussion

Animal models play a crucial role in advancing cancer research as they provide indispensable means for replicating genetic and pathophysiological factors that contribute significantly to cancer development [19, 20]. Moreover, these models offer valuable opportunities to assess novel therapeutic strategies in pre-clinical settings by utilizing disease-specific oncologic models. Among the various options available, rodents are commonly employed in such studies due to their lightweight characteristics, ease of breeding, and cost-effectiveness compared to larger animal counterparts. In particular, mice have emerged as a favored choice in cancer research due to the ready availability of genetically modified strains, allowing targeted investigations into the underlying mechanisms of cancer [19–22].

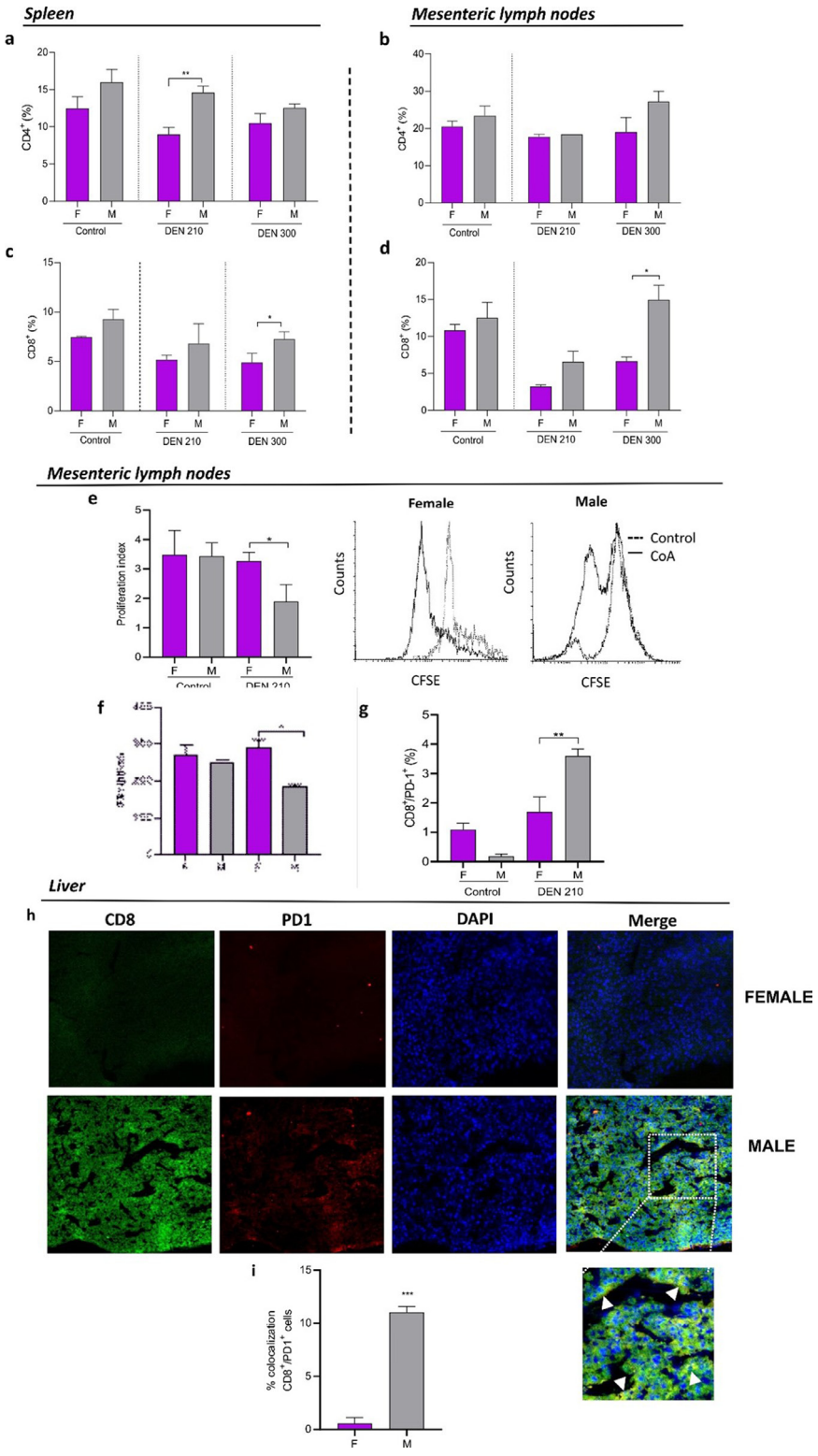

Fig. 4. T lymphocytes in liver, spleen, and mesenteric lymph nodes of male and female diethylnitrosamine (DEN) − treated C3H mice. Percentage of CD4+ T lymphocytes in the spleen (a) and lymph node (b), and percentage of CD8+ T lymphocytes in the spleen (c) and lymph node (d) from female or male control mice, and DEN-treated C3H mice. (e) Proliferation index of CD8+ T lymphocytes and representative CFSE flow cytometric histograms of lymph nodes from female or male control and DEN-treated C3H mice (f) IFN-γ concentration in the supernatant of CD8 T lymphocyte cultures of lymph nodes from female or male control and DEN − treated C3H mice evaluated by ELISA assay. (g) Percentage of PD-1+ in CD8+ T lymphocytes of lymph nodes from female or male control mice and DEN-treated C3H mice. Results are expressed as mean ± SEM of percentage (%) of cells. n=5 mice per group were used. **P*<0.05; ***P*<0.01. All statistical analyses of this figure were performed using ANOVA followed by the Tukey test. F=female; M=male. (h) Representative immunofluorescence showing colocalization between CD8 lymphocytes (green) and PD-1 (red). (i) Signal overlap was quantified using MBF-Image J. Pearson's colocalization coefficients were calculated from three independent experiments and then converted to percentages (****P*<0.001).

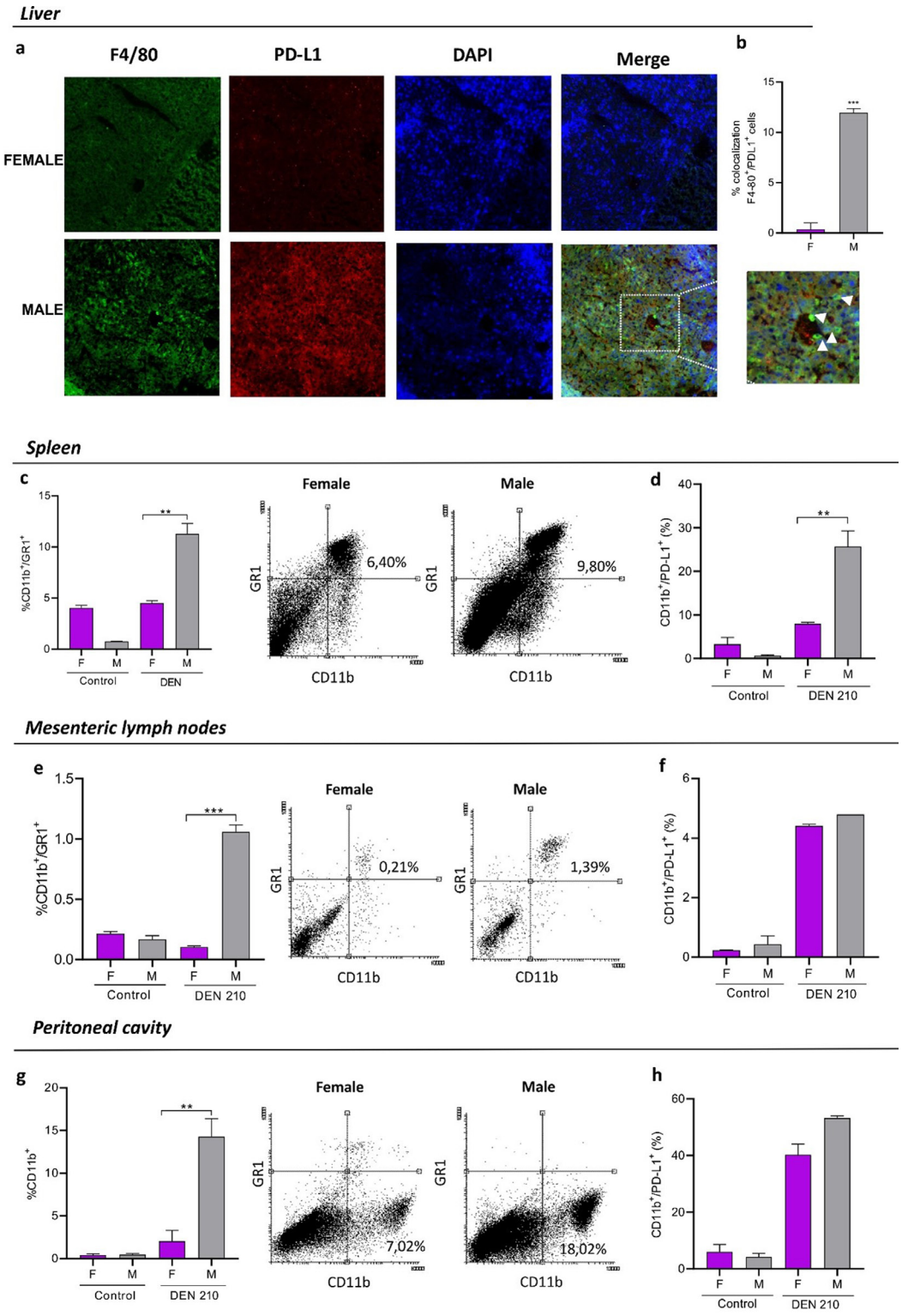

Fig. 5. Myeloid cells in the liver, mesenteric lymph nodes, spleen, and peritoneum of female and male C3H mice 210 days after administration of the carcinogen DEN. Mice were euthanized by cervical dislocation at 210 days post-DEN administration. The liver, spleen, and mesenteric lymph nodes were removed. Peritoneal lavages with PBS-5% fetal bovine serum was performed. Cell populations were evaluated by immunofluorescence (a, b) and flow cytometry (c–h). (a) Representative immunofluorescence showing colocalization between F480 macrophages (green) and PD-L1 (red) in the liver. (b) Signal overlap was quantified using MBF-Image J. Pearson's colocalization coefficients were calculated from three independent experiments and then converted to percentages (***P<0.001). (c–h) Percentage of myeloid cells CD11b+/GR1+, and representative dot plots of myeloid cell population in the spleen (c), mesenteric lymph nodes (e), and peritoneal cavity (g) of female or male DEN-treated C3H mice 210 days after administration of the carcinogen. Percentage of myeloid cells that express PD-L1 in the spleen (d), mesenteric lymph nodes (f), and peritoneal cavity (h) of DEN-treated C3H mice. Results are expressed as mean ± SEM. n=5 mice per group were used in the representative experiment. **P<0.01. ***P<0,001. All statistical analyses of this figure were performed using ANOVA followed by the Tukey test. F=female; M=male.

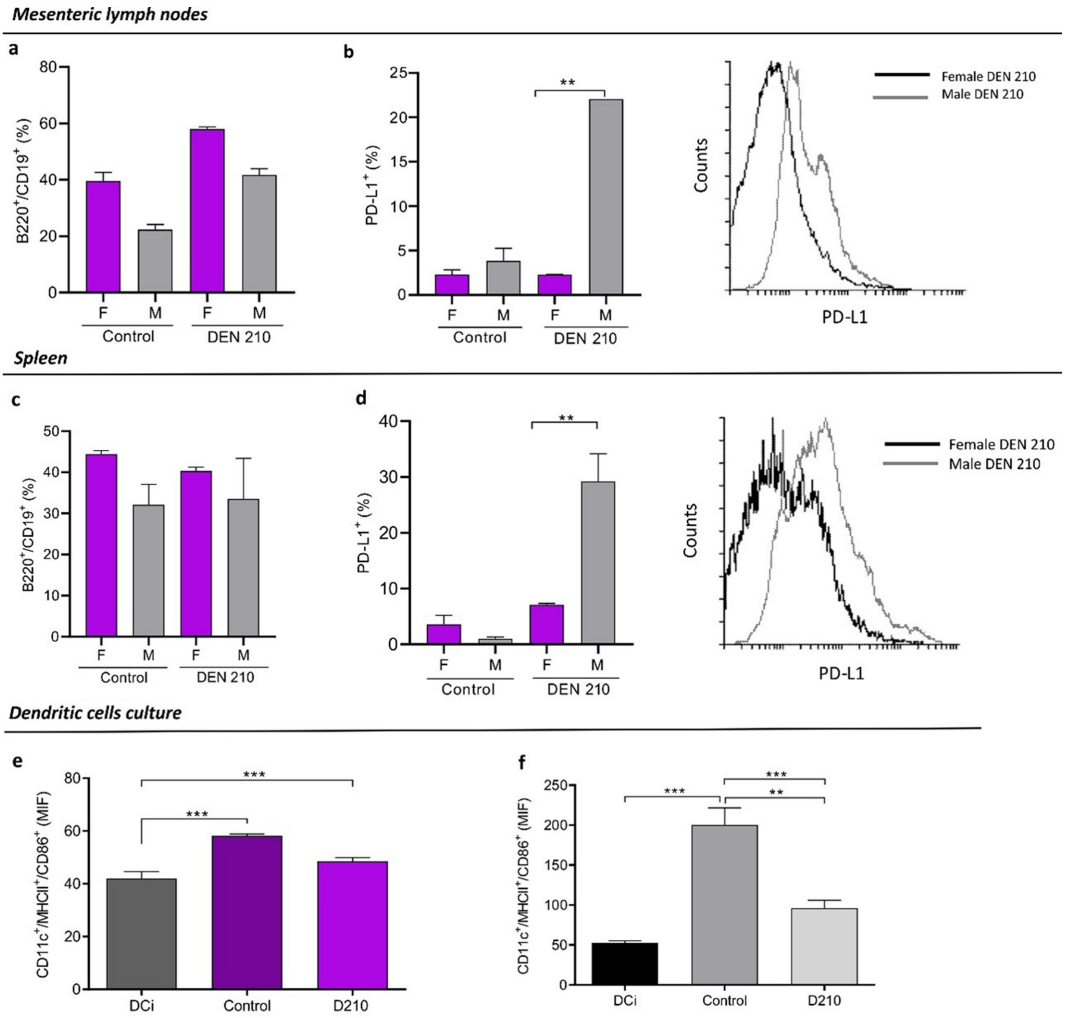

Fig. 6. B lymphocytes and dendritic cells (DC)*in vitro* maturation of female and male diethylnitrosamine (DEN) − treated C3H mice. Mice were euthanized by cervical dislocation 210 days post-DEN administration. The liver, spleen, and mesenteric lymph nodes were removed. Cell populations were evaluated by flow cytometry. (a, c) Percentage of CD19+/B220+ B lymphocytes in mesenteric lymph node (a) and spleen (c) from female and male DEN-treated C3H mice 210 days after administration of the carcinogen. (b, d) Percentage of B lymphocytes that express PD-L1+, and representative histograms in mesenteric lymph nodes (b) and spleen (d) of DEN-treated C3H mice. Results are expressed as mean ± SEM. (e, f) Expression of cell-surface receptors MHCII and CD86 in bone marrow-derived $CD11c^+$ DC stimulated with liver lysates, evaluated by flow cytometry. Negative controls were unstimulated DC (DCi), and positive controls were DC stimulated with 5 μg/ml LPS. Results are expressed as mean ± SEM. n=5 mice per group were used in the representative experiment. ***P*<0.01. ****P*<0,001. All statistical analyses of this figure were performed using ANOVA followed by the Tukey test. MFI=mean fluorescence intensity. F=female; M=male.

In recent years, a range of rodent models have been established for studying hepatocellular carcinoma (HCC). Assessing the extent to which mouse models accurately replicate the characteristics observed in human counterparts can pose challenges in many instances. In terms of sex disparity, HCC exhibits a three to fivefold higher propensity to develop in males compared to females [23–25]. The importance of including females in experimental designs becomes apparent when considering this marked contrast [1, 3, 4].

One of the most used models is diethylnitrosamine (DEN)-induced HCC in C3H mice that produce multiple tumor foci per liver that gradually increase over time and progress to trabecular hepatocellular metastatic carcinomas. This model has histology, genetic signature, and sex disparity similar to human HCCs [1].

In this paper, confirming data from former publications [1, 2, 4], we observed that following administration of the carcinogen DEN, females exhibited a higher incidence of hyperplasias and adenomas compared to males. Remarkably, unlike their male counterparts, females did not exhibit progression to HCC in nearly all cases. While the liver damage induced by DEN has been extensively investigated in male mice [1, 2, 10] it is

worth noting that the response in females differs significantly and has been much less studied.

In our study, we focused on two distinct time points: days 210 and 300 post-DEN administration. At day 210, males exhibited a distorted hepatic architecture without signs of necrosis, with hepatic adenomas being the predominant feature, indicating a stage preceding the development of HCC. In contrast, our observations in female mice revealed a reduced distortion of tissue architecture, a lower pro-inflammatory profile and a notably lower percentage of liver senescent areas. At day 300 post-DEN, while tumors have progressed to HCC in males, they predominantly remain as adenomas in females.

These observations are in line with previous reports highlighting that the persistent production of IL-6 by Kupffer cells plays a crucial role in the pathogenesis of DEN-induced HCC and, on the other hand, estrogen-mediated downregulation of IL-6 secretion may contribute to a decreased incidence of HCC in female mice. Subsequently, since IL-6 creates a positive feedback loop that progressively increases the pathological effect of the senescence/inflammatory microenvironment, differential hormonal-mediated secretion of IL-6 between males and females would be associated with the resistance exhibited by females towards the progression of HCC [6, 8, 9].

It is important to note that differences in IL-6 levels between sexes were also observed in older control mice. Untreated female mice consistently showed low levels of IL-6 throughout aging, unlike males, suggesting a potential resistance of females against the development of certain pro-inflammatory conditions associated with aging, which could delay tumor development. The association between elevated IL-6 levels, aging, and tumor development has been documented in various tumor models [26–30].

Furthermore, the relationship between inflammation and immunosuppression has been previously documented in DEN-treated male mice [31–33]. The interactions between cancer and immune cells have been studied in some clinical and experimental settings, providing insights into the crosstalk between malignant cells, and cells of innate and adaptive immunity. Besides, tumor cells develop complex and varied strategies to evade detection and destruction by immune cells, primarily by favoring the generation of immunosuppressive cells such as regulatory T cells or myeloid-derived suppressor cells [34]. Previous studies have demonstrated that macrophages within the tumor microenvironment can facilitate HCC growth through the surface expression of PD-L1, which promotes the establishment of an immunosuppressive microenvironment, predominantly influenced by pre-existing activated CD8+ T cells that typically exhibit an exhausted phenotype characterized by heightened PD-1 expression [35–37]. However, whether the PD-L1/PD-1 axis exhibits sex-specific characteristics contributing to enhanced tumor resistance in females remains unexplored. We showed that the immune response to DEN-induced HCC differs between female and male C3H mice. In our study, a lower expression of PD-1 was observed in CD8 T lymphocytes, as well as a lower expression of PD-L1 in hepatic macrophages, myeloid cells, and infiltrating B lymphocytes in the spleen and lymph nodes of DEN-treated females. These differences could contribute, at least in part, to the delay in the progression from adenomas to HCC observed in females, unlike what occurs in males.

In summary, although the use of male mice is usually recommended to reduce the number of experimental mice in this model [1], studies focused on females are fruitful for future investigation. In effect, sex disparity in the induction, growth, and progression of DEN-induced HCC could be associated with a differential expression of both immunologic as well as non-immunologic anti-tumor mechanisms, suggesting that more accurate comparative studies between resistant and more susceptible hosts might help to unveil novel therapeutic strategies against cancer.

Authors' Contributions

DM performed most of the experiment and helped in writing and correcting the main manuscript text. MT and AB helped in the accomplishment of some experiments. MV collaborated with some experiments on Figs. 4 and 5. OB helped in the realization *of in vivo* experiments. GP and RT performed the processing and analysis of liver samples for histopathology. AD and RR designed and supervised all experiments and drafted the manuscript.

Data Availability Statement

All data generated or analyzed during this study are included in this published article and its supplementary information files.

Conflict of Interest

The authors declare that they have no financial and non-financial competing interests.

Ethics Approval and Consent to Participate

All methods were according to the NIH Guide for the Care and Use of Laboratory Animals. All experimental protocols were approved by the Committee for the Care and Use of Laboratory Animals (CICUAL) of Instituto de Medicina Experimental (IMEX-CONICET, protocol N°087/2021). All methods were performed following ARRIVE guidelines.

Funding

This work was supported by Instituto Universitario en Ciencias de la Salud, Fundación H. A. Barceló (BA-MED-119) and PICT START UP 2019-00018.

References

1. Tolba R, Kraus T, Liedtke C, Schwarz M, Weiskirchen R. Diethylnitrosamine (DEN)-induced carcinogenic liver injury in mice. Lab Anim. 2015; 49:(Suppl): 59–69. [Medline] [CrossRef]
2. Connor F, Rayner TF, Aitken SJ, Feig C, Lukk M, Santoyo-Lopez J, et al. Mutational landscape of a chemically-induced mouse model of liver cancer. J Hepatol. 2018; 69: 840–850. [Medline] [CrossRef]
3. Maronpot RR. Biological basis of differential susceptibility to hepatocarcinogenesis among mouse strains. J Toxicol Pathol. 2009; 22: 11–33. [Medline] [CrossRef]
4. Liu S, Huang F, Ru G, Wang Y, Zhang B, Chen X, et al. Mouse models of hepatocellular carcinoma: classification, advancement, and application. Front Oncol. 2022; 12: 902820. [Medline] [CrossRef]
5. Sung H, Ferlay J, Siegel RL, Laversanne M, Soerjomataram I, Jemal A, et al. Global cancer statistics 2020: GLOBOCAN estimates of incidence and mortality worldwide for 36 cancers in 185 countries. CA Cancer J Clin. 2021; 71: 209–249. [Medline] [CrossRef]
6. Nakatani T, Roy G, Fujimoto N, Asahara T, Ito A. Sex hormone dependency of diethylnitrosamine-induced liver tumors in mice and chemoprevention by leuprorelin. Jpn J Cancer Res. 2001; 92: 249–256. [Medline] [CrossRef]
7. Rao KV, Vesselinovitch SD. Age- and sex-associated diethylnitrosamine dealkylation activity of the mouse liver and hepatocarcinogenesis. Cancer Res. 1973; 33: 1625–1627. [Medline]
8. Naugler WE, Sakurai T, Kim S, Maeda S, Kim K, Elsharkawy AM, et al. Gender disparity in liver cancer due to sex differences in MyD88-dependent IL-6 production. Science. 2007; 317: 121–124. [Medline] [CrossRef]
9. Prieto J. Inflammation, HCC and sex: IL-6 in the centre of the triangle. J Hepatol. 2008; 48: 380–381. [Medline] [CrossRef]
10. Goldfarb S, Pugh TD, Koen H, He YZ. Preneoplastic and neoplastic progression during hepatocarcinogenesis in mice injected with diethylnitrosamine in infancy. Environ Health Perspect. 1983; 50: 149–161. [Medline] [CrossRef]
11. Ma L, Nidadavolu LS, Yang H, Langdon J, Westbrook R, Tsui BMW, et al. Targeted deletion of interleukin-6 in a mouse model of chronic inflammation demonstrates opposing roles in aging: Benefit and harm. J Gerontol A Biol Sci Med Sci. 2021; 76: 211–215. [Medline] [CrossRef]
12. Cao X, Zhang Y, Zhou Q, Sun S, He M, Wang X, et al. Establishment of a novel mouse hepatocellular carcinoma model for dynamic monitoring of tumor development by bioluminescence imaging. Front Oncol. 2022; 12: 794101. [Medline] [CrossRef]
13. Smith D, Anderson D, Degryse AD, Bol C, Criado A, Ferrara A, et al. Classification and reporting of severity experienced by animals used in scientific procedures: FELASA/ECLAM/ESLAV Working Group report. Lab Anim. 2018; 52:(1_suppl): 5–57. [Medline] [CrossRef]
14. Schneider CFT. Adaptive immunity suppresses formation and progression of diethylnitrosamine-induced liver cancer. Physiol Behav. 2018; 176: 139–148.
15. Thoolen B, Maronpot RR, Harada T, Nyska A, Rousseaux C, Nolte T, et al. Proliferative and nonproliferative lesions of the rat and mouse hepatobiliary system. Toxicol Pathol. 2010; 38:(Suppl): 5S–81S. [Medline] [CrossRef]
16. Hernandez-Segura A, Nehme J, Demaria M. Hallmarks of cellular senescence. Trends Cell Biol. 2018; 28: 436–453. [Medline] [CrossRef]
17. Chiarella P, Vulcano M, Bruzzo J, Vermeulen M, Vanzulli S, Maglioco A, et al. Anti-inflammatory pretreatment enables an efficient dendritic cell-based immunotherapy against established tumors. Cancer Immunol Immunother. 2008; 57: 701–718. [Medline] [CrossRef]
18. Montagna DR, Duarte A, Chiarella P, Rearte B, Bustuoabad OD, Vermeulen M, et al. Inhibition of hyperprogressive cancer disease induced by immune-checkpoint blockade upon cotreatment with meta-tyrosine and p38 pathway inhibitor. BMC Cancer. 2022; 22: 845. [Medline] [CrossRef]
19. De Minicis S, Kisseleva T, Francis H, Baroni GS, Benedetti A, Brenner D, et al. Liver carcinogenesis: rodent models of hepatocarcinoma and cholangiocarcinoma. Dig Liver Dis. 2013; 45: 450–459. [Medline] [CrossRef]
20. Obeid M, Khabbaz R, Garcia K, Schachtschneider K, Gaba R. Translational animal models for liver cancer. Am J Interv Radiol. 2018; 2: 1–7. [CrossRef]
21. Shetty S, Sharma N, Ghosh K. Epidemiology of hepatocellular carcinoma (HCC) in hemophilia. Crit Rev Oncol Hematol. 2016; 99: 129–133. [Medline] [CrossRef]
22. Yang JD, Roberts LR. Management of combined hepatocellular carcinoma-cholangiocarcinoma. Curr Hepatol Rep. 2018; 17: 385–391. [Medline] [CrossRef]
23. Kumari R, Sahu MK, Tripathy A, Uthansingh K, Behera M. Hepatocellular carcinoma treatment: hurdles, advances and prospects. Hepat Oncol. 2018; 5: HEP08. [Medline] [CrossRef]
24. Greten TF, Papendorf F, Bleck JS, Kirchhoff T, Wohlberedt T, Kubicka S, et al. Survival rate in patients with hepatocellular carcinoma: a retrospective analysis of 389 patients. Br J Cancer. 2005; 92: 1862–1868. [Medline] [CrossRef]
25. Atwa SM, Odenthal M, El Tayebi HM. Genetic heterogeneity, therapeutic hurdle confronting sorafenib and immune checkpoint inhibitors in hepatocellular carcinoma. Cancers (Basel). 2021; 13: 1–18. [Medline] [CrossRef]
26. Kim IH, Xu J, Liu X, Koyama Y, Ma HY, Diggle K, et al. Aging increases the susceptibility of hepatic inflammation, liver fibrosis and aging in response to high-fat diet in mice. Age (Dordr). 2016; 38: 291–302. [Medline] [CrossRef]
27. Gomez CR, Karavitis J, Palmer JL, Faunce DE, Ramirez L, Nomellini V, et al. Interleukin-6 contributes to age-related alteration of cytokine production by macrophages. Mediators Inflamm. 2010; 2010: 475139. [Medline] [CrossRef]
28. Ershler WB, Keller ET. Age-associated increased interleukin-6 gene expression, late-life diseases, and frailty. Annu Rev Med. 2000; 51: 245–270. [Medline] [CrossRef]
29. Liu H, Shen J, Lu K. IL-6 and PD-L1 blockade combination inhibits hepatocellular carcinoma cancer development in mouse model. Biochem Biophys Res Commun. 2017; 486: 239–244. [Medline] [CrossRef]

30. Nenu I, Toadere TM, Topor I, Țichindeleanu A, Bondor DA, Trella ȘE, et al. Interleukin-6 in hepatocellular carcinoma: a dualistic point of view. Biomedicines. 2023; 11: 2623. [Medline] [CrossRef]
31. Refolo MG, Messa C, Guerra V, Carr BI, D'Alessandro R. Inflammatory mechanisms of HCC development. Cancers (Basel). 2020; 12: 641. [Medline] [CrossRef]
32. Yu LX, Ling Y, Wang HY. Role of nonresolving inflammation in hepatocellular carcinoma development and progression. NPJ Precis Oncol. 2018; 2: 6. [Medline] [CrossRef]
33. Giraud J, Chalopin D, Blanc JF, Saleh M. Hepatocellular carcinoma immune landscape and the potential of immunotherapies. Front Immunol. 2021; 12: 655697. [Medline] [CrossRef]
34. Salemme V, Centonze G, Cavallo F, Defilippi P, Conti L. The crosstalk between tumor cells and the immune microenvironment in breast cancer: implications for immunotherapy. Front Oncol. 2021; 11: 610303. [Medline] [CrossRef]
35. Ma J, Zheng B, Goswami S, Meng L, Zhang D, Cao C, et al. $PD1^{Hi}$ $CD8^{+}$ T cells correlate with exhausted signature and poor clinical outcome in hepatocellular carcinoma. J Immunother Cancer. 2019; 7: 331. [Medline] [CrossRef]
36. Dudek M, Pfister D, Donakonda S, Filpe P, Schneider A, Laschinger M, et al. Auto-aggressive $CXCR6^{+}$ CD8 T cells cause liver immune pathology in NASH. Nature. 2021; 592: 444–449. [Medline] [CrossRef]
37. Hao L, Li S, Deng J, Li N, Yu F, Jiang Z, et al. The current status and future of PD-L1 in liver cancer. Front Immunol. 2023; 14: 1323581. [Medline] [CrossRef]